Coaxial to Empty Substrate Integrated Waveguide Transition for Small Satellite Technology

Laura Rivero [(1)], David Herraiz[(1)], Héctor Esteban[(1)], Santiago Cogollos [(1)], and Vicente E. Boria[(1)]
lrivmir@teleco.upv.es, daherza@teleco.upv.es, hesteban@upv.es, sancobo@dcom.upv.es, vboria@dcom.upv.es
Institute of Telecommunications and Multimedia Applications. Universitat Politècnica de València. Spain

***Abstract*—Empty Substrate Integrated Waveguides (ESIW) integrate hollow 3D waveguides into printed circuit boards (PCBs), thereby creating an empty waveguide with reduced height while maintaining low cost, low profile, and easy integration. Several transitions have been proposed to connect ESIW circuits to microstrip lines. However, these transitions generally increase the complexity of the manufacturing process and cannot be directly connected to measurement equipment. Therefore, in this communication, a direct coaxial-to-ESIW transition based on magnetic coupling is proposed. This structure can be manufactured with reduced complexity, requiring only simple cuts and metalization. An equivalent circuit model has been proposed, which provides initial values for the transmission parameters, and reduces the optimization time by 20%.**

I. Introduction

Low Earth orbit (LEO) satellites serve as a compelling illustration of the evolving landscape in space communications [1]. These new low-cost satellite generations facilitate rapid data transfer and global connectivity. Within this context, the C-band spectrum (4-8 GHz) has gained popularity in satellite communications and is increasingly used for small satellites [2]. The development of small satellites requires the creation of new, cost-effective, highly integrated, and high-performance technologies.

One solution to meet these requirements in the emerging scenario is the Substrate Integrated Waveguide (SIW) [3]. This technology integrates a 3D waveguide using dielectric substrates, resulting in cost-effective fabrication, seamless integration into printed circuit boards (PCB), and compact solutions. However, the dielectric losses increase the total insertion losses of these microwave components, and electrical performance is still not sufficient for some applications.

In response to this drawback, the Empty SIW (ESIW) was presented in [4], where the electromagnetic wave is propagated through the air. ESIW microwave components do offer improved performance compared to their SIW counterparts, showcasing superior characteristics in terms of losses and quality factors, albeit with a slight increase in size.

Several transitions from planar technologies to ESIW have been proposed to achieve seamless integration. These transitions typically involve connecting a microstrip line to the ESIW, using various matching elements such as dielectric tapers or widening sections [5], [6]. However, many industrial microwave components, especially active ones like standard state power amplifiers (SSPAs) or measurement equipment, require a coaxial connector. Thus, to connect these elements, several intermediate transitions are necessary (coaxial-to-microstrip and microstrip-to-ESIW), thereby increasing manufacturing complexity and insertion losses. In addition, these transitions incorporate both metalized and non-metalized elements, thereby increasing the manufacturing complexity.

Therefore, to achieve a more seamless integration, this paper proposes a direct coaxial to ESIW transition. The solution eliminates the need for intermediate transitions, achieving substrate independence and enhancing overall efficiency while reducing manufacturing complexity.

II. Proposed structure

The ESIW is built by emptying one substrate, metalizing the lateral walls, and then assembling a top and a bottom metallic layer using tin soldering paste. As shown in Fig. 1, the height of the emptied central layer is h, which in this work has been chosen to be 1.6 mm, which corresponds to a commercial and cost-effective FR-4 substrate. The resulting waveguiding structure, the ESIW, is low cost and low profile, and since the waves propagate through a closed and empty channel, there have very low radiation and propagating losses.

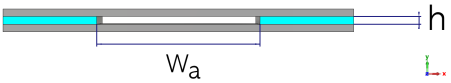

Fig. 1: Transversal section of the ESIW.

The chosen ESIW width (see Fig. 1), W_a, is 34.8488 mm, which corresponds to that of a standard WR137 rectangular waveguide, whose recommended (monomode) operating frequency ranges from 5.85 to 8.2 GHz, that is, in the C-band.

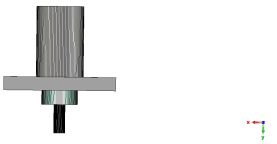

Fig. 2: Front view of the SMA connector.

To introduce the signal from the coaxial line into the ESIW, the proposed transition consists of placing an SMA connector (see Fig. 2) on the top layer of the ESIW, just in the middle of the ESIW channel width (see Fig. 3). Then, the inner conductor of the SMA connector is threaded inside the ESIW until it reaches the bottom ESIW layer. Circular perforations are made and metalized in both the top and bottom layers of the ESIW, ensuring that the inner conductor of the SMA connector completely passes through the hole in the top layer of the ESIW without touching it. If that happened, the SMA connector would be shot-circuited, and all the signal would be reflected in the coaxial cable and would not enter the ESIW.

Finally, the SMA inner conductor is soldered to the bottom layer, securing a robust and reliable connection within the ESIW structure, as shown in Fig. 3. This electrical connection of the coaxial inner conductor to the bottom ESIW metallic cover, provides a main magnetic coupling between the coaxial and ESIW field distributions.

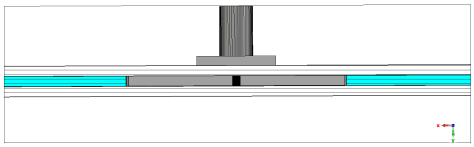

Fig. 3: ESIW and SMA connector.

In order to accomplish a good impedance matching, and to ensure that the signal injected in the ESIW is not reflected and returned to the coaxial cable, the ESIW is terminated with a shot-circuit (flat solid conducting wall, see Fig. 4) on one end of the ESIW, at a convenient distance from the place where the SMA connector is inserted. If that distance is chosen correctly, the signal that comes from the coaxial cable screwed to the SMA connector will be properly injected into the ESIW, and this signal will propagate as the fundamental mode of the ESIW (TE_{10} mode) in the opposite direction of the ESIW short circuit.

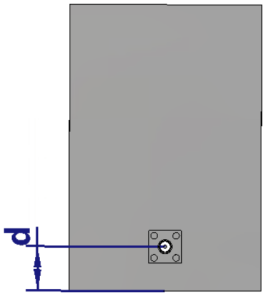

Fig. 4: Top view of the ESIW, where d is the distance between the SMA and the short-circuited wall.

The appropriate distance between the SMA connector and the ESIW short-circuited end will depend on where the maximum of the magnetic field is located, since the excitation is carried out through magnetic coupling. Magnetic coupling has been chosen as the preferred excitation method for the proposed structure, primarily because the structure comprises layers with a total height of only 1.6 mm each. This limited height makes it impractical to achieve excitation through electric coupling, which requires a probe with a smaller length than the height of the ESIW structure. Thus, the proposed assembly technique facilitates seamless cable integration, maintaining signal integrity while ensuring a stable and efficient transmission path through the waveguide.

Once the new structure has been proposed, the only design parameter is the distance from the SMA insertion point in the ESIW to the short-circuited ESIW end (d). This distance has to be chosen after an optimization process that iterates until the distance that maximizes the return losses is found. In order to speed up this optimization process, it is convenient to use an adequate equivalent circuit of the proposed transition that can be simulated and optimized faster than with a full-wave electromagnetic (EM) simulation of the real 3D structure.

III. Equivalent Circuit Model

In an effort to expedite the optimization process and establish an initial starting point without prolonged computational delays, alternative and simplified models for the structure were explored. The objective was to find a tool that can efficiently handle the optimization task, and provide an initial design without the time-intensive nature of a full-wave EM software tool, such as computer simulation technology (CST) [7].

After exploring several possibilities, a circuit model based on [8] was adopted. In this model, as illustrated in Fig. 5, the transition is represented as a T-circuit formed by two capacitors and an inductor in series with the coaxial characteristic impedance.

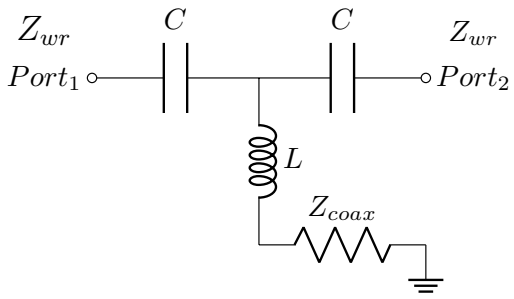

Fig. 5: T circuit equivalent model for the SMA connected to the ESIW, where Z_{wr} and Z_{coax} correspond to the impedances of the rectangular waveguide and the coaxial line.

The equivalent circuit of Fig. 5 models the transition of the SMA connector and the considered ESIW. The inductor models the main magnetic coupling effect that the inner SMA conductor produces in the ESIW. It is well known that a through H-plane cylinder inside a rectangular waveguide can be modeled as a lumped inductor. The capacitors model any parasitic electric coupling that can appear between the inductive post and the lateral walls, although this effect is very weak and thus the value of the capacitors is expected to be very high, almost as if they were short-circuited. Finally, the lumped inductor is connected to the coaxial cable, modeled in the equivalent circuit with its characteristic impedance Z_{coax}.

This coaxial characteristic impedance (Z_{coax}) depends solely on the inner (b) and outer (a) radius of the coaxial line (standard commercial measurements, see Fig. 6), and the relative permittivity of the dielectric material between the two conductors of the coaxial (ϵ_r), according to the following expression,

$$Z_{coax} = \frac{60}{\sqrt{\epsilon_r}} \ln\left(\frac{a}{b}\right) \tag{1}$$

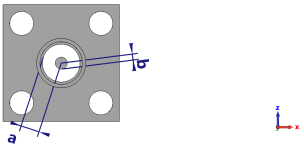

Fig. 6: Dimensions of the SMA connector.

In this case, the material is Teflon, therefore $\epsilon_r = 2.1$. The SMA connector adopted for this transition is the R125.414.000 commercial version, whose outer radius (a) is 2.03 mm and the inner radius (b) is 0.64 mm (see Fig. 6). The frequency range covered by the proposed connector goes from 0 to 24 GHz, with the upper limit being higher than the maximum operating frequency of the considered ESIW (8.2 GHz).

Once an equivalent circuit for the SMA connected to the ESIW is obtained, the equivalent circuit is completed connecting an empty ESIW section ended with a short-circuit on one side, and the characteristic impedance of the ESIW (where the power is injected) on the other side, as shown in Fig. 7.

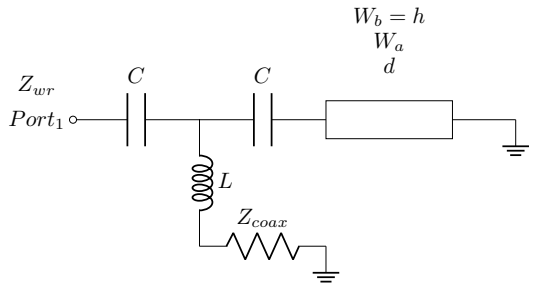

Fig. 7: Equivalent T circuit model for the SMA connected to the ESIW with width W_a, height $W_b = h$, considering on one side a short-circuited ESIW of length d.

The characteristic circuital impedance of the ESIW can be computed according to different criteria, since the propagating mode in the ESIW is not a TEM mode. The modal impedance for the transversal electric mode (TE), which is indeed the only impedance that can be defined unambiguously, is expressed as follows,

$$Z_{TE} = \frac{120\pi}{\sqrt{1 - \left(\frac{f_c}{f}\right)^2}} \tag{2}$$

where f_c is the cut-off frequency of the fundamental TE_{10} mode:

$$f_c = \frac{c}{2\,W_a} \tag{3}$$

c is the speed of light in vacuum, and W_a is the width of the ESIW.

There are three different possible definitions for the circuital impedance of the ESIW: power-voltage, voltage-current, and power-current [9]. We have chosen the same definition used in the CST commercial simulator, so the resulting S parameters of the equivalent circuit will be directly comparable to those of CST software tool.

According to ref. [9], the power-voltage circuit impedance is defined as follows,

$$Z_{pv} = 2\frac{h}{W_a} Z_{TE} \tag{4}$$

where h and W_a are the height and width of the ESIW (as it is defined in Fig. 1).

The initial values for L and C can be determined by using expressions for an inductive post located inside a rectangular waveguide, as outlined in [9]. Alternatively, these values can be obtained using the following expressions provided in [10],

$$j\frac{X_a}{Z_{pv}} = \frac{2S_{21}}{(1 - S_{11}^2) - S_{21}^2} \tag{5}$$

$$-j\frac{X_b}{Z_{pv}} = \frac{1 + S_{11} - S_{21}}{1 - S_{11} + S_{21}} \tag{6}$$

where X_a and X_b correspond to the reactances ($X_a \rightarrow j\omega L$, $X_b \rightarrow 1/(j\omega C)$), and Z_{pv} the power-voltage circuit impedance (see equation.4). In (5) and (6), S_{11} and S_{21} denote the S parameters of a lossless symmetric two-port network with an inductive post in the central plane of discontinuity of a waveguide, where the values of these parameters S can be obtained using the CST tool. Thus, the values of L and C for any real structure can be computed using (5) and (6). In our case, the initial value of L was calculated for an operational frequency of $f_0 = 6$ GHz, resulting in a value of $L = 0.37$ nH. On the other hand, the value of C tends to infinity, due to the higher distance between the inductive post and the lateral walls of the waveguide. Both the equivalent circuit of Fig. 7 and the proposed transition have been simulated, using Matlab [11], and CST [7].

An initial value of $\lambda_g/4$ has been considered for the distance d (from the SMA connector to the short-circuited end of the ESIW), where λ_g corresponds to the guide wavelength calculated following the equation.

$$\lambda_g = \frac{\lambda}{\sqrt{1 - \left(\frac{f_c}{f_0}\right)^2}} \tag{7}$$

where f_0 = 6 GHz, f_c is the cut-off frequency described in (3) and λ is the well-known free-space wavelength, described by this equation,

$$\lambda = \frac{c}{f_0} \tag{8}$$

being c is the speed of light in vacuum and f_0 = 6 GHz.

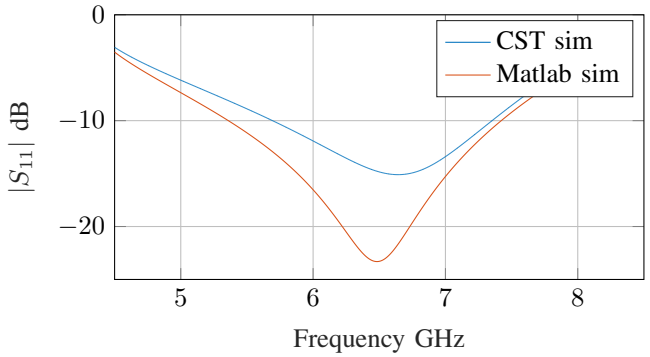

Fig. 8: Comparison between the reflection coefficient of the transition in CST and Matlab after optimizing the values of L and C with $d = \lambda_g/4$.

The inductance (L) and capacitance (C) values of the equivalent circuit were optimized (using the initial values aforementioned), to conveniently match the results for the reflection coefficient of the transition provided by CST, with those obtained from the equivalent circuit with Matlab. The optimized value for L was 0.3839 nH, whereas the optimized capacitance of the capacitance tends toward infinity

(C = 50,000 pF), allowing its removal from the equivalent circuit, leaving only the inductor and the coaxial characteristic impedance. Fig. 8 shows the reflection coefficients that have been obtained using both CST and Matlab, considering the optimized values of L and C for the equivalent circuit of Fig. 5 and with $d = \lambda_g/4$.

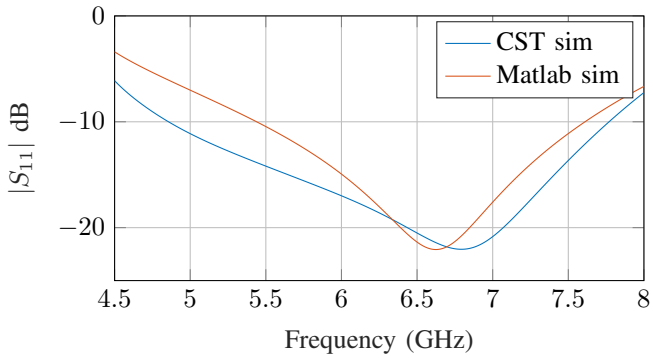

Fig. 9: Comparison between the reflection coefficient of the transition with CST and Matlab (equivalent circuit considering the optimized values of L and C) and optimizing distance d.

As shown in Fig. 8, a perfect matching between CST and Matlab is not achieved for the entire frequency range, but the coincidence is good enough for the equivalent circuit to provide a good approximation to the real transition.

As already mentioned, the results have been obtained using an initial distance d, from the SMA connector to the short-circuited end of the ESIW, of $\lambda_g/4$. In order to improve the impedance matching, d is then optimized obtaining the results of Fig. 9.

The optimization described takes $d = \lambda_g/4 = 17.9$ mm in both CST and Matlab as an initial value. The optimization in Matlab takes 22 seconds with the Nelder-Mead Simplex optimization algorithm after 535 iterations. CST, with the same optimization algorithm and goal function, takes 29 minutes and 8 seconds. Afterwards, and taking the optimized value of Matlab as the initial value for other optimization in CST, it can be observed that the optimization in CST with a best initial value takes less time than with $\lambda_g/4$. These results are collected in Table I.

	Matlab	CST	CST
Frequencies	5.5-7.5 GHz	5.5-7.5 GHz	5.5-7.5 GHz
Goal	$\|S11\| < -20$dB	$\|S11\| < -20$dB	$\|S11\| < -20$dB
Algorithm	Simplex	Simplex	Simplex
Time	22 s	29 min 8 s	23 min
Initial d	17.9 mm	17.9 mm	17.2 mm
Optimized d	17.2 mm	16.9 mm	17 mm

TABLE I: Comparison between CST and Matlab optimization processes.

The procedure using the equivalent circuit for obtaining a good initial point for CST enabled a more efficient optimization process, reducing the computational time by 20% compared with an optimization process using only CST.

IV. Conclusions

In this communication, a direct coaxial to ESIW transition has been proposed. The solution is based on a short-circuited ESIW with the SMA inner conductor passing through the ESIW and being soldered to the bottom layer. To accelerate the design procedure, an equivalent circuit of the transition has been proposed to efficiently obtain an initial starting point for further optimization with a full-wave EM software tool. This approach has expedited the optimization process, saving 20% of the computation time. Despite the fact the proposed equivalent circuit does not perfectly match the response of the real structure (in a wide frequency range), it is good enough to be used to obtain an initial good solution for the proposed transition, to be further optimized with a full-wave EM simulator.

Acknowledgements

This work has been funded by the Ministerio de Ciencia, Innovación y Universidades (MICIU) and the European Union (EU) through the projects PID2022-136590OB-C41 and TED2021-129196B-C41 (grants MICIU/AEI/10.13039/501100011033/ FEDER, UE and MICIU/AEI/10.13039/501100011033/ UE NextGenerationEU/PRTR).

References

[1] M. N. Sweeting, "Modern small satellites-changing the economics of space," *Proceedings of the IEEE*, vol. 106, no. 3, pp. 343–361, 2018.

[2] P. Thakker and W. Shiroma, *Emergence of Pico- and Nanosatellites for Atmospheric Research and Technology Testing*, ser. Progress in astronautics and aeronautics. American Institute of Aeronautics and Astronautics, 2010. [Online]. Available: https://books.google.es/books?id=cBRicAAACAAJ

[3] D. Deslandes and K. Wu, "Integrated microstrip and rectangular waveguide in planar form," *Microwave and Wireless Components Letters, IEEE*, vol. 11, no. 2, pp. 68–70, Feb. 2001.

[4] A. Belenguer, H. Esteban, and V. E. Boria, "Novel empty substrate integrated waveguide for high-performance microwave integrated circuits," *IEEE Transactions on Microwave Theory and Techniques*, vol. 62, no. 4, pp. 832–839, April 2014.

[5] H. Esteban, A. Belenguer, J. R. Sánchez, C. Bachiller, and V. E. Boria, "Improved low reflection transition from microstrip line to empty substrate-integrated waveguide," *IEEE Microwave and Wireless Components Letters*, vol. 27, no. 8, pp. 685–687, Aug 2017.

[6] Z. Liu, J. Xu, and W. Wang, "Wideband transition from microstrip line-to- empty substrate-integrated waveguide without sharp dielectric taper," *IEEE Microwave and Wireless Components Letters*, vol. 29, no. 1, pp. 20–22, Jan 2019.

[7] Dassault Systèmes, "Computer Simulation Technology (CST)." [Online]. Available: http://www.cst.com

[8] A. Suntives and R. Abhari, "Transition structures for 3-d integration of substrate integrated waveguide interconnects," *IEEE Microwave and Wireless Components Letters*, vol. 17, no. 10, pp. 697–699, Oct 2007.

[9] N. Marcuvitz, *Waveguide handbook*. IET, 1951, no. 21.

[10] Y. Leviatan, P. Li, A. Adams, and J. Perini, "Single-post inductive obstacle in rectangular waveguide," *IEEE Transactions on Microwave Theory and Techniques*, vol. 31, no. 10, pp. 806–812, Oct 1983.

[11] "MATLAB," MathWorks. [Online]. Available: https://www.mathworks.com/products/matlab.html